JOURNAL OF AIRCRAFT
Vol. 34, No. 5, September–October 1997

Numerical Study on the Underexpanded Coanda Jet

Keisuke Sawada* and Kengo Asami†
Tohoku University, Sendai 980-77, Japan

The problem of Coanda jet flow in an underexpanded supersonic environment is studied numerically by solving the Navier–Stokes equations in two and three dimensions. The study considers a flow initiated by a jet bounded by a sidewall and expanding around a circular cylinder, for which a set of experimental data exists. Pressure distributions on the cylinder surface are compared in detail with the experimental data. In the two-dimensional calculation, the characteristic oscillatory pressure pattern is reproduced well, but quantitative agreement with the experimental data is rather poor. The three-dimensional calculation reveals the significant influence of the sidewall on the flowfield. It is suggested that the three-dimensional structure developed in the flowfield is the cause of the poor quantitative agreement obtained in the two-dimensional calculation.

Nomenclature

A	=	height of the nozzle throat
E, F, G	=	convective flux functions in each coordinate direction
E_v, F_v, G_v	=	viscous flux functions in each coordinate direction
P_r	=	ratio of the total pressure of the jet to the ambient static gas
Q	=	conservative variable
R	=	radius of the cylinder
X	=	upper wall extension from the throat
X/A	=	ratio of the upper wall extension to the nozzle height
y	=	spanwise coordinate in three-dimensional calculation ($y = 0$:center of jet flow, $y = \pm 1$:sidewall)
θ	=	angle from the throat

Introduction

IT is well known that the lift of an aircraft's wing is increased greatly if a jet flow is blown backward from a narrow, long slit located on the upper surface of a wing near the rounded trailing edge. The jet flows along the curved surface to the trailing edge because of an effect termed Coanda. The phenomenon occurs because the jet flow increases the circulation around the wing. The airfoil thus becomes a so-called circulation control airfoil in this case.[1–3]

Another way to augment a lift force is to put a jet engine directly on the wing and blow a jet along the upper surface. Again, because of the Coanda effect, the jet turns its direction along the wing surface without separating from it.[4,5] It is known as the upper surface blowing technique and has been utilized in several experimental short takeoff and landing aircraft.

The usefulness of the Coanda effect has been known to the aeronautical engineering community since the 1950s, and has received considerable attention since then.[6,7] However, the Coanda effects were rather confined to the jet flows in the incompressible regime; i.e., where the ratio of the total pressure of the jet to the ambient atmosphere was relatively small.

The most serious problem in the engineering application of the Coanda effect is the jet flow detachment from the curved Coanda surface. It has been reported that the geometry of the jet exhaust has a significant influence over the position of the jet flow detachment, that setting a splitter plate at the nozzle lip is effective in suppressing the detachment, and that the jet flow is likely to be detached if the height of the jet throat is large in relation to the radius of the cylinder.[6–8]

In one of the few supersonic Coanda jet studies made to date, the work of Bevilaqua and Lee[9] examined the effect of geometry of the exhaust nozzle. They tried to design a vortex nozzle to produce a radial velocity superimposed on the axial velocity, in the hopes of making the Coanda jet flow attach farther to the curved surface. A convergent–divergent nozzle geometry was reported to be useful for that purpose.

Recently, an experimental study was conducted with a Coanda jet flow with a high total pressure underexpanded along a circular cylinder.[10] It reported that the jet flow detachment could be delayed considerably by employing a convergent–divergent nozzle.

The jet flow detachment from the curved surface occurs because of the shock–boundary-layer interaction involving the shock waves produced inside the jet plume; therefore, it is a result of a high static pressure at the nozzle exit. By lowering the exhaust static pressure through the use of a divergent nozzle, the jet flow detachment can be slowed.

The numerical investigations of the Coanda jet flow reported so far have considered only the utilization of circulation control airfoils with mostly subsonic jet flows; furthermore, they were mostly two dimensional. The three-dimensional Coanda jet flow in the compressible regime, such as the underexpanded supersonic case, deserves greater attention because of its large potential benefit in engineering applications. The primary purpose of the present study is to try to understand the structure of the underexpanded supersonic Coanda jet and to develop a suitable numerical method for simulating the Coanda jet flow accurately.

First, we conduct two-dimensional Navier–Stokes simulations in which we try to reproduce the experimental pressure distributions along the cylindrical surface.[10] In these calculations, we employ not only the two different schemes, an implicit scheme and an explicit one, but also two different turbulence models, the conventional algebraic model and the one-equation model. We are particularly interested in the possible influence of the turbulence model and mesh geometry on the quantitative description of the flowfield. Three-dimensional

Presented as Paper 96-1936 at the AIAA 27th Fluid Dynamics Conference, New Orleans, LA, June 17–20, 1996; received Sept. 9, 1996; revision received March 31, 1997; accepted for publication April 8, 1997.

*Associate Professor, Department of Aeronautics and Space Engineering. Senior Member AIAA.

†Graduate Student, Department of Aeronautics and Space Engineering; currently Engineer, Mitsubishi Motor Ltd., Hashime-cho, Okazaki 444, Japan.

calculations are then carried out to see the influence of the sidewall on the overall structure of the flowfield.

In the following text, we present the numerical methods, and then describe the geometry of the flowfield. The results obtained both in two- and three-dimensional calculations are presented and discussed. Finally, we give the conclusions obtained in the course of the present study.

Numerical Methods

Here we briefly describe the numerical methods used in the present study. The governing equations are the conventional Reynolds-averaged Navier–Stokes equations, both in two- and three-dimensional spaces, as

$$\frac{\partial Q}{\partial t} + \frac{\partial (E - E_v)}{\partial x} + \frac{\partial (F - F_v)}{\partial y} + \frac{\partial (G - G_v)}{\partial z} = 0 \qquad (1)$$

In the two-dimensional case, z-derivative terms are neglected. An ideal gas equation of state is employed, and the constant ratio of the specific heats is assumed to be 1.4 throughout the flowfield. A thin-layer approximation is used in the evaluation of the viscous terms.

We solve the governing equations by two different numerical schemes. The first (hereafter called scheme A) is an implicit finite volume upwind total variation diminishing (TVD) scheme using Roe's approximate Riemann solver.[11] For solving the viscous high Reynolds number flows, we employ the Baldwin–Lomax algebraic turbulence model.[12] The lower/upper–alternating direction implicit (LU–ADI) factorization method[13] is used for an implicit time integration.

The other method (hereafter called scheme B) is a cell-group splitting explicit finite volume upwind TVD scheme.[14] It employs Goldberg's one-equation turbulence model,[15] which does not involve the distance from the nearby solid wall. The computational efficiency of an explicit time integration is improved by using the cell-group splitting time integration technique, which is similar to the conventional zone-splitting method. The whole flowfield is divided into a maximum of four cell groups.

Although this cell-group splitting method was originally developed to facilitate unsteady flow simulations, it is also applicable to steady flow if we simultaneously employ the local time-stepping method. Because of space limitations, we will not describe the details of this approach in this paper. The cell-group splitting approach also works quite well in the unstructured mesh system.

Computational Conditions

In the calculation, we consider the same flowfield as in the experimental setup we intend to simulate.[10] A schematic illustration for a two-dimensional case is given in Fig. 1. In the calculation, we assume $R = 2$, $A = 0.1$, and $X/A = 5$.

Note that the geometry of the circulation control airfoil corresponds to the case with $X = 0$. In the circulation control airfoil, a converging nozzle geometry is usually employed, since the total pressure of the jet flow is not so high and the sonic condition is seldom reached at the throat. With a higher total pressure, as in the present study, the sonic condition is likely achieved and, hence, the divergent section is needed for further expansion. This divergent geometry is easily given by employing the upper wall extension (Fig. 1).

We consider the following two experimental conditions: in case A, we assume $P_r = 5.07$; whereas $P_r = 7.17$ in case B. The Reynolds number is 3.2×10^4, based on the nozzle height. The Mach number at the jet exit varies, depending on the mesh geometry, which will be described later. In the experiment,[10] the height to the lateral width of the jet throat (aspect ratio) was as large as 20, so that the two-dimensional properties are likely to hold, at least at the center of the jet flow. The upper wall region of the jet nozzle is modeled simplistically by a splitter plate, because the flow above the plate is static and, therefore, does not influence the jet flow.

The computational meshes for the two-dimensional calculation are shown in Fig. 2. The structured mesh shown in Fig. 2a has 181×101 grid points, covering θ up to 180 deg from the throat (hereafter called mesh 2A). For this mesh, a sonic inflow condition with uniform velocity profile is given at the throat.

To see the possible influence of the inflow boundary condition, we use another mesh in which a settling chamber region is appended to mesh 2A. It has 202×101 grid points. A magnified view of the chamber region is shown in Fig. 2b (hereafter called mesh 2B). The settling chamber is designed to reduce the inflow Mach number as low as 0.1. Although we again specify the uniform inflow there, the boundary layers are allowed to develop along the chamber walls, resulting in a realistic velocity profile at the sonic throat. For a mesh convergence study, we employ a fine mesh having the same geometry as mesh 2A, but doubled the number of grid points in each coordinate direction.

In the three-dimensional calculation, on the other hand, we consider only one mesh system. In Fig. 3a, a schematic illustration of the computational domain is shown. The geometry of the spanwise cross section coincides with mesh 2B (with a settling chamber), and there are 135×62 grid points in each cross section. Sidewalls are assumed to be at the side lips of

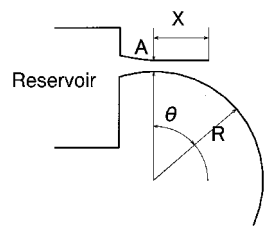

Fig. 1 Experimental setup.[10]

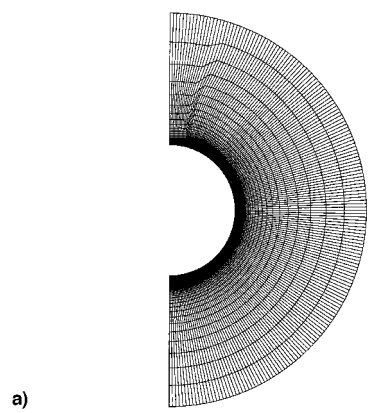

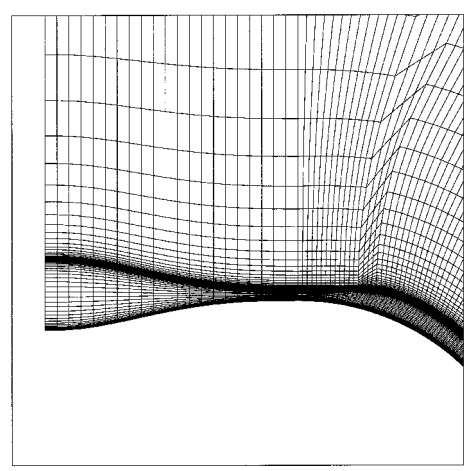

Fig. 2 Meshes for two-dimensional calculations: a) whole view of mesh 2A (181 × 101) and b) settling chamber region of mesh 2B (202 × 101).

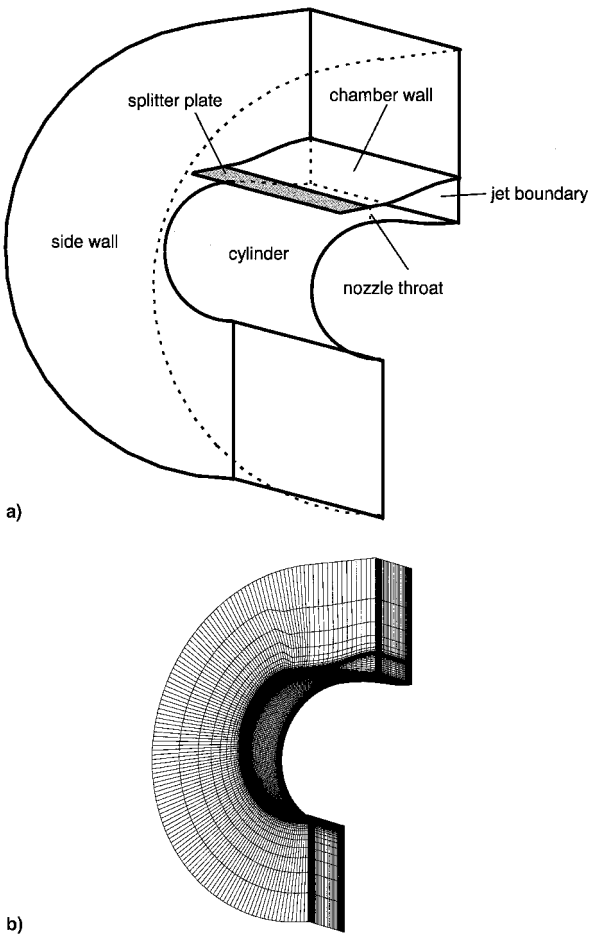

Fig. 3 Mesh for three-dimensional calculations: a) schematic illustration (splitter plate is highlighted) and b) whole view of three-dimensional mesh (135 × 101 × 62) (splitter plate is not shown).

the jet exit and are treated as nonslip walls. The aspect ratio of the jet exit, as stated earlier, is 20. We have 101 grid points in the spanwise direction. We solve the full span of the jet flow without assuming any symmetry. Figure 3b shows a typical example of the present mesh.

The boundary conditions for two-dimensional calculations are as follows: the nonslip boundary condition is applied to the cylinder surface as well as to the splitter plate. Other boundaries, except the inflow, are treated as ambient. As the initial condition for two-dimensional calculations, the ambient static state is given to all of the computational cells. In some test calculations, we initially assumed the jet column to be along the curved surface to avoid the initial violent state near the trailing edge of the upper wall extension. The final state was found to be independent of the choice of initial conditions.

The boundary condition for the three-dimensional calculations are basically the same as in the two-dimensional cases, except at the sidewalls where the nonslip boundary condition is enforced. As the initial condition for the three-dimensional calculations, we first obtain the two-dimensional solution in one spanwise cross section and then assign it to all the cross sections.

As noted earlier, only the static ambient atmosphere is considered in the present study. The matching condition at the jet boundary becomes quite complicated if we have a freestream flow around the cylinder. Because the freestream also flows along the curved jet boundary, the pressure gradient in the radial direction is yielded, resulting in the lower matching pressure at the jet boundary and, hence, in the higher effective pressure ratio at the nozzle exit. Furthermore, the matching pressure depends on the shape of the jet boundary. These effects make the prediction of jet flow detachment more difficult in case of a circulation control airfoil.

Calculated Results

Two-Dimensional Cases

At first, we examine the two-dimensional results for case A ($P_r = 5.07$). Figure 4a shows the Mach number distribution for the entire flowfield obtained by scheme A (implicit scheme with Baldwin–Lomax turbulence model), using mesh 2A. The jet expands in the divergent nozzle and is ejected in the downstream region. The peak Mach number in the first jet cell is as large as 2.34. The interval of the Mach contours is 0.1. Therefore, at the nozzle exit, the Mach number is about 1.9. As the jet flows downstream, the boundary layer on the cylinder surface develops and the mixing layer at the jet boundary rapidly grows. The size of the jet core caught between the boundary and mixing layers gradually shrinks in the downstream region along the cylinder.

Figure 5 shows the normalized pressure distribution on the cylinder surface together with the experimental data. In the first expansion/compression cellular region (hereafter called a jet–cell), calculated result shows a reasonable agreement with the experimental data. However, as in the farther downstream region, the deviation from the experimental data becomes significant. The amplitude of the calculated pressure oscillations decays at the slower rate than the experiment, and the phase of the oscillations is also retarded.

The same flowfield is calculated by scheme B (explicit scheme with the Goldberg turbulence model[15]), using mesh 2A. The Mach number contours are shown in Fig. 4b, and the surface pressure distribution is in Fig. 5. In this result, the

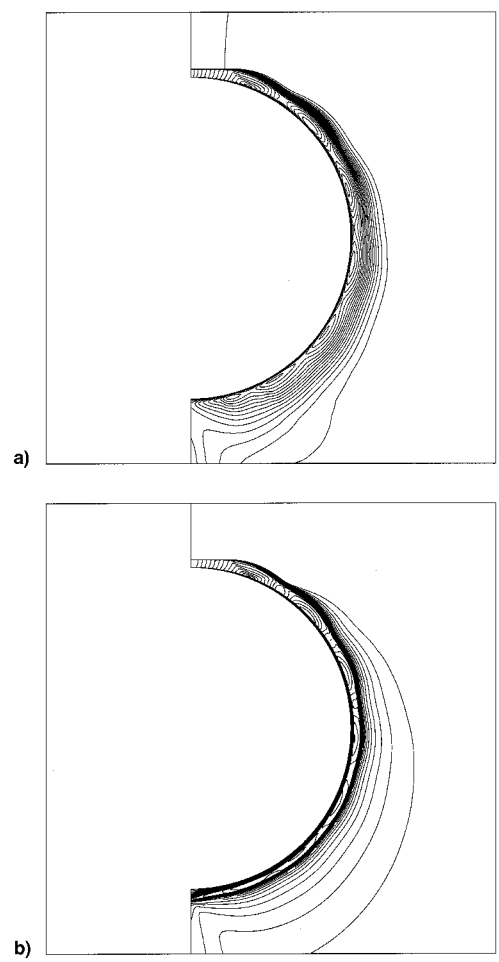

Fig. 4 Calculated Mach number contours for case A using mesh 2A. Schemes a) A and b) B.

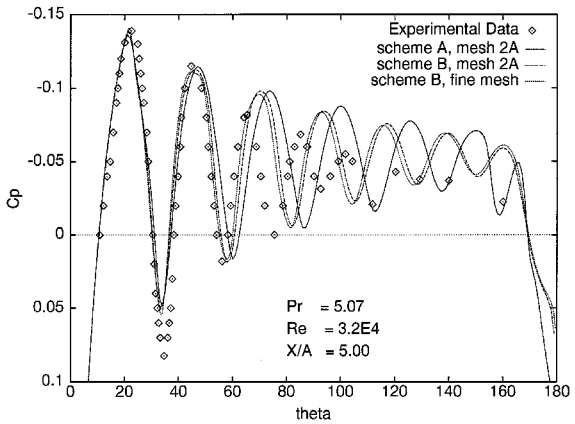

Fig. 5 Comparison of surface pressure distributions for case A.

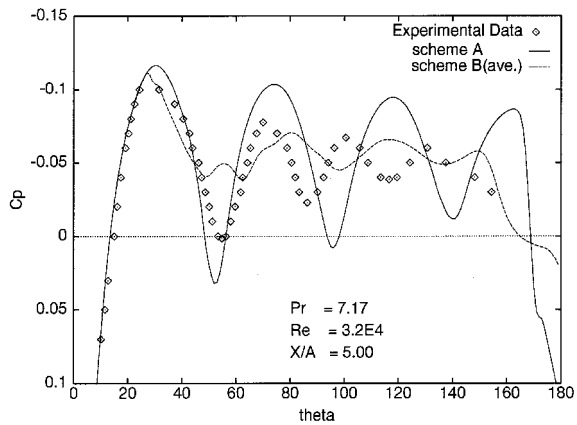

Fig. 6 Comparison of surface pressure distributions for case B.

amplitude of the pressure oscillations decays slightly faster than the scheme A result, and the coincidence with the experiment is improved.

As a mesh convergence study, we solve the same case by scheme B, using a fine mesh. The obtained pressure distribution is plotted also in Fig. 5. The overall pressure distribution coincides reasonably well with the coarse result. All of the important features of the flowfield are well reproduced with mesh 2A.

Now, let us consider case B, in which the pressure ratio is $P_r = 7.17$. The surface pressure distribution obtained by scheme A using mesh 2A is shown in Fig. 6. In this case, the quantitative agreement with the experimental data becomes poor. Even in the first jet–cell, the deviation of the pressure distribution is obvious in the compression phase. Furthermore, the jet–cell structure clearly remains at $\theta = 180$ deg, and the decay rate of the amplitude of oscillations differs considerably.

The same flowfield is again calculated by scheme B, using the same computational mesh. In this calculation, the flowfield did not reach a steady state, but significantly fluctuated. Therefore, we turned to the time-accurate calculation and obtained the ensemble average of the solution with over 18,000 samples. The surface pressure distribution for this averaged flowfield is shown in Fig. 6.

In the scheme B result, the boundary-layer separation takes place at the compression phase in the first jet–cell. The amplitude of the pressure oscillations is significantly suppressed because of the separation, and becomes closer to the experimental data, although we still have large phase errors. The separation of the boundary layer is probably caused by the insufficient development of a turbulent boundary layer at the first jet–cell. It is assumed that the uniform inflow condition applied to the sonic throat is responsible for this separation.

To see whether this is really the case, we carried out the same calculations using mesh 2B (with a settling chamber). Because the uniform inflow condition is applied at a location far upstream from the sonic throat, the boundary layer is already fully developed at the sonic throat. Figure 7a shows the surface pressure distribution for case A ($P_r = 5.07$), obtained by scheme B. Because of the augmented viscous effect in the boundary layer, the amplitude of the pressure oscillations decays slightly faster than that of the mesh 2A result. In other words, the enhancement of viscous effect in this case results in a better quantitative agreement with the experiment.

In the case B calculation ($P_r = 7.17$), using mesh 2B, we could not obtain the steady solution and, therefore, we again turned to the time-accurate calculation. The boundary-layer separation in this case takes place in the far downstream region. The averaged surface pressure distribution is plotted in Fig. 7b.

It should be noted that, once the boundary layer attaches in the first jet–cell because of the enhanced viscous effect, a large

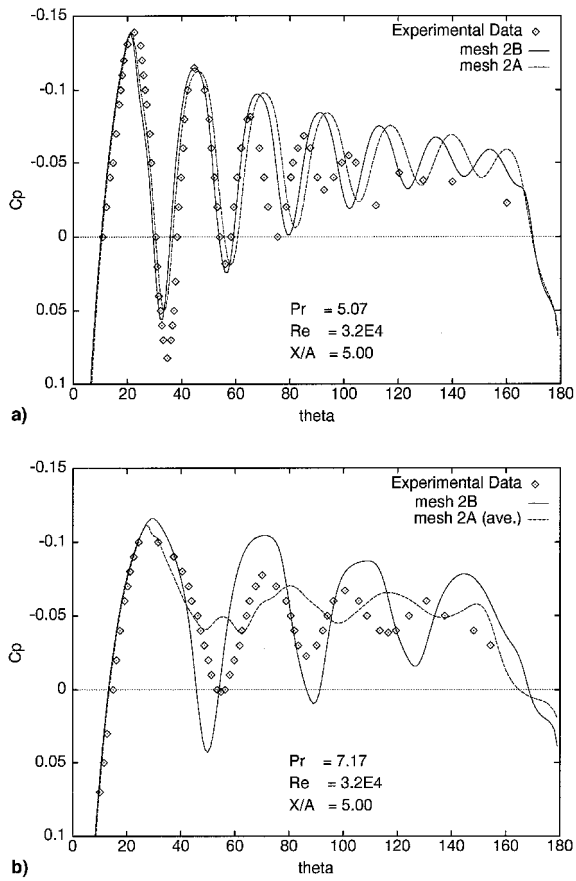

Fig. 7 Surface pressure distributions obtained by scheme B using mesh 2B.

amplitude of the pressure oscillations recovers. It resembles the scheme A result, which is far different from the experimental data. Therefore, we are now in a contradictory situation where the viscous effect should be enhanced for obtaining a faster decay of the pressure oscillations in case A; whereas it should be decreased to have a boundary-layer separation in case B.

Three-Dimensional Cases

All of the three-dimensional calculations are carried out by scheme B. We obtained converged solutions for case B as well as for case A. We assume that this convergence in case B was obtained by the coarser mesh used in the three-dimensional calculation.

Let us examine the case A result first. Figure 8 shows the Mach number contours in the midplane, which is between the cylinder surface and the splitter plate, and is parallel with the cylinder surface. One can clearly see that the lateral extent of the jet core region exhibiting the jet–cell structure gradually shrinks, and the perturbations from the sidewalls penetrate toward the center of the jet flow, as in the downstream region.

Figure 9 shows the limiting surface streamlines on the cylinder surface, as well as on the sidewall. We can find separation lines corresponding to the jet–cell structure. The secondary flows are first initiated as the downward flows (toward the center of cylinder) on the sidewall, because of the imbalance of the pressure gradient and the centrifugal force. Inward-directed secondary flows (toward the center of the jet flow) are then induced on the cylinder surface along the separation lines, and a longitudinal vortex is generated at the corner accordingly.

The surface pressure distribution at the center of the jet flow is plotted in Fig. 10. It shows a reasonable agreement with the two-dimensional result when $\theta < 80$ deg. However, in the farther downstream region, the amplitude of oscillations does not decay monotonically, and eventually shows a small peak at $\theta \sim 130$ deg. This seems to be caused by the collapsing jet core in the lateral direction, which two-dimensional calculation cannot take into account. One can see that the agreement with the experimental data at this position is still poor.

If, on the other hand, we plot the pressure distributions at the off-center positions, the agreement is drastically improved. The pressure distributions at the selected off-center positions are also shown in Fig. 10. At $y = -0.5511$, we obtain a fairly good agreement with the experimental data in terms of the peak values of the pressure oscillations at the expansion region, and also the phase of the oscillations for the first four jet–cells.

Now, let us examine the case B result. Figure 11 shows the Mach number contours in the midplane parallel to the cylinder surface. We can observe that the significant perturbations are generated periodically according to the jet–cell structure near sidewalls. The limiting surface streamlines for case B are shown in Fig. 12. Again, we can find separation lines clearly

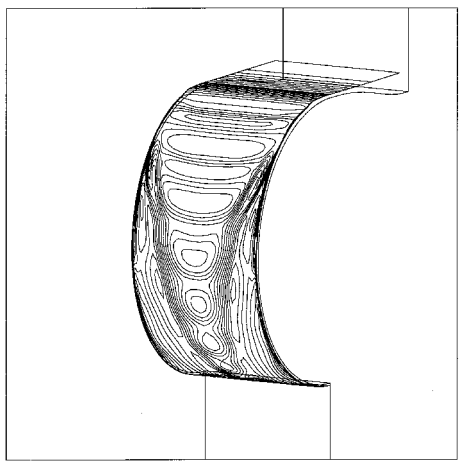

Fig. 8 Mach number contours in midplane parallel to the cylinder surface for case A.

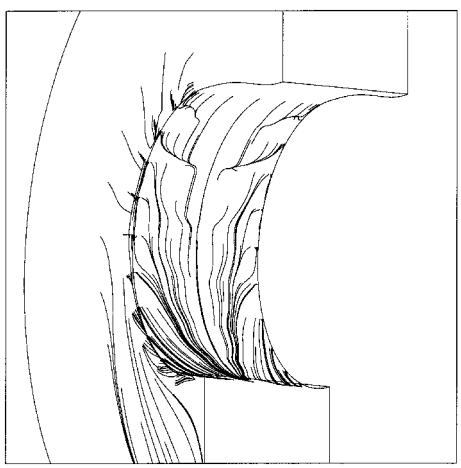

Fig. 9 Limiting surface streamlines on the cylinder surface as well as on the sidewall for case A.

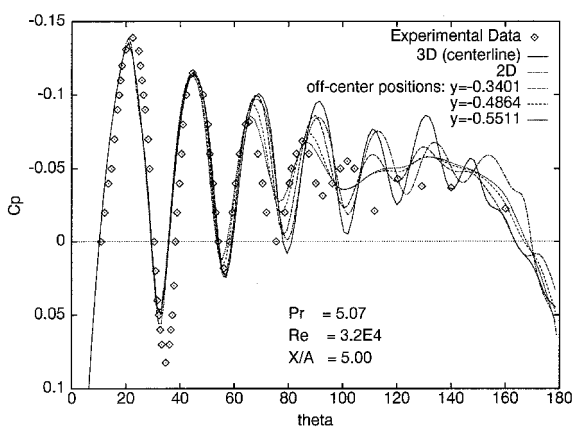

Fig. 10 Surface pressure distributions for case A.

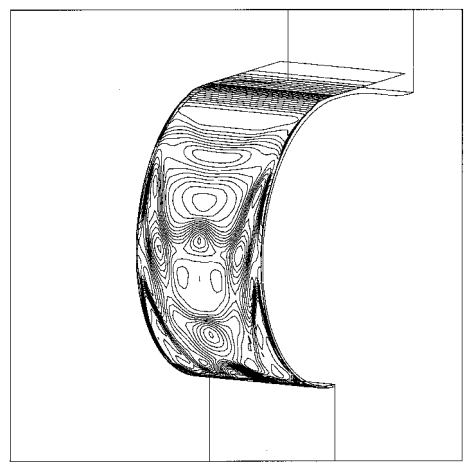

Fig. 11 Mach number contours in midplane parallel to the cylinder surface for case B.

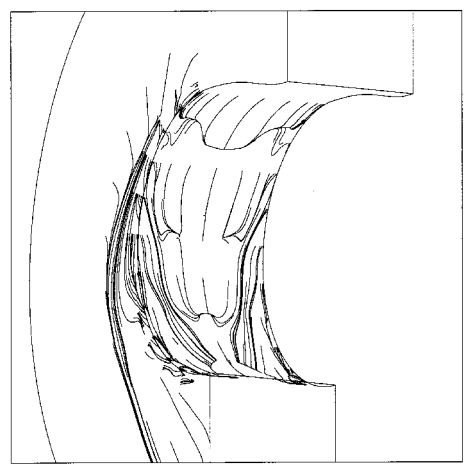

Fig. 12 Limiting surface streamlines on the cylinder surface as well as on the sidewall for case B.

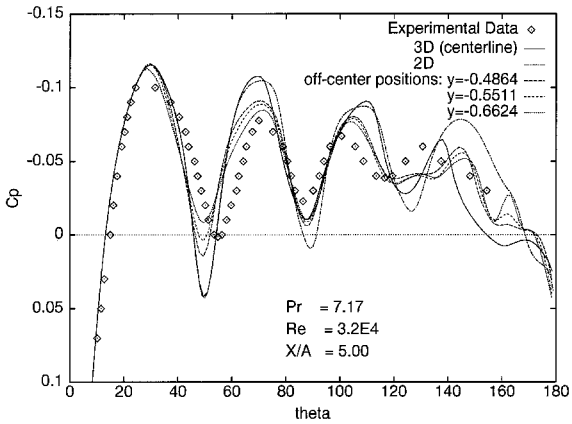

Fig. 13 Surface pressure distributions for case B.

on the cylinder surface corresponding to the jet–cell structure. The secondary flows on the cylinder surface are also directed toward the center of the jet flow.

The surface pressure distribution at the center of the jet flow, as well as at the selected off-center positions, are shown in Fig. 13. As in the case A result, it resembles the two-dimensional result at the center of the jet flow, and the coincidence with the experimental data is still poor. However, the coincidence is again greatly improved at the off-center positions.

Discussions

The underexpanded supersonic Coanda jet is characterized by the jet–cell structure with a diminishing jet core. The flowfield is highly dominated by a turbulent boundary layer as well as turbulent mixing, and this fact makes the numerical simulation more difficult for a quantitative comparison.

The two-dimensional results for case A (P_r = 5.07) can be summarized as follows: in the first two jet–cells, the surface pressure distribution shows a reasonable agreement with the experimental data, whereas discrepancies become evident in the far downstream region. The coincidence in the downstream region is slightly improved if we employ scheme B, and it is further improved if we use mesh 2B to enhance the viscous effect in the boundary layer. As far as examining these results, one is tempted to say that the disagreement in the downstream region is caused by the inadequate development of boundary and mixing layers, which neither turbulence model could properly provide for.

The case B results (P_r = 7.17) of two-dimensional calculations, however, are contrary to this supposition. We observe that the amplitude of the surface pressure oscillations differs considerably with the experimental data, so far as the boundary layer in the first jet–cell adhering to the cylinder surface, whereas this amplitude resembles the experiment if the boundary-layer separation takes place. Thus, the enhancement of viscous effect leads to suppression of the boundary-layer separation, which results in an inferior quantitative agreement with the experiment.

It is found that this conflicting situation can be resolved in the three-dimensional simulations. The three-dimensional calculations carried out so far show that the marked three-dimensional structure develops in the flowfield, even for the present geometry of the jet exit, with an aspect ratio as large as 20. The boundary-layer separation takes place at the compression phase of the jet–cell, in both cases A and B. The surface streamline plots show that the boundary layer is likely to be separated near the corner region, where a corner vortex develops accordingly. In other words, the boundary-layer separation is more likely to occur than the two-dimensional calculation.

The surface pressure distribution changes considerably, depending on the lateral position; we actually obtain an improved agreement with the experimental result at those off-center positions, where the effect of boundary-layer separation becomes significant. The amplitude of the surface pressure oscillations are notably reduced by the boundary-layer separation, which is consistent with the two-dimensional result for case B (Fig. 6).

It is therefore suggested that the development of the three-dimensional structure in the flowfield is the possible cause of the poor agreement with the experimental data obtained in the two-dimensional calculations. Note that, however, the agreement with the experimental data at the center of the jet flow was yet as poor as in the two-dimensional result. Is it then possible to obtain an accurate prediction along the center of the jet flow if we have a larger boundary-layer separation? If this is the case, how can we obtain such a boundary-layer separation? These are questions yet to be answered.

It has been reported that a convergent–divergent nozzle geometry can provide significant improvement of the Coanda jet performance.[10] The experimental data in that reference showed that the jet flow detachment occurred far earlier with a simple converging nozzle geometry because of the oblique shock wave developed in the jet plume. A converging nozzle only allows the jet flow to expand up to the sonic condition, and the resulting pressure at the jet exit may be much higher than the ambient pressure. At the nozzle lip, strong expansion waves are then generated that lead to the formation of an oblique shock wave after the reflection at the jet boundary. This oblique shock wave not only lifts off the boundary layer from the cylinder surface because of the adverse pressure gradient, but also tends to deflect the streamlines upward from the surface.[10] Contrary to this, even for a higher total pressure ratio, the use of a convergent–divergent nozzle geometry can nearly equal the pressure of the ambient gas at the nozzle exit. This avoids the formation of expansion waves and, hence, the possible shock waves. The boundary layer is then less likely to be separated and, thus, the performance can be increased.

Use of a divergent nozzle geometry, however, is a more or less two-dimensional idea, in the sense that the flowfield is considered to be two dimensional for obtaining a matching condition. We have shown in the present study that a significant three-dimensional structure inevitably develops in the flowfield, which may critically affect the detachment of the jet flow from the Coanda surface. The computational fluid dynamics (CFD) method developed in the present study can be used as a practical engineering tool to examine the flowfield in detail, and help to find the possible remedy for the detachment problem.

Establishing a sophisticated design method for a nozzle geometry utilizing the Coanda effect has yet to be accomplished. A new design procedure based on the genetic algorithm may be a candidate. Such an approach certainly requires the highly accurate and reliable analysis method of the flowfield, and we expect that the present CFD method will be useful in such applications.

Conclusions

In the present study, we carried out the numerical simulations of the underexpanded supersonic Coanda jet flows in two and three dimensions, and obtained the following conclusions:

1) The characteristic pattern of the pressure distribution on the cylinder surface is generated by the successive jet–cell structures that are forced to decay by the development of a turbulent boundary layer, mixing layer, and separated corner flow.

2) Only in the upstream region near the splitter plate do two-dimensional simulations give close agreement with experimental data. This distinction becomes evident in the far downstream region, regardless of the scheme and computational mesh used in the calculation.

3) Three-dimensional structure of the flowfield is found to be dominant in the far downstream region, which is caused by the boundary-layer separation and the associated corner vortex.

The surface pressure distribution at the off-center position shows an improved quantitative agreement with the experimental data. This suggests that the existence of the significant three-dimensional structure in the flowfield is the cause of the poor quantitative agreement obtained in the two-dimensional calculation.

Acknowledgment

This work was supported, in part, by a Scientific Research on Priority Areas, Grant-in-Aid 06231201, from the Ministry of Education, Science and Culture in Japan.

References

[1]Shrewsbury, G. D., "Numerical Study of a Research Circulation Control Airfoil Using Navier-Stokes Methods," *Journal of Aircraft*, Vol. 26, No. 1, 1989, pp. 29–34.

[2]Williams, S. L., and Franke, M. E., "Navier-Stokes Methods to Predict Circulation Control Airfoil Performance," *Journal of Aircraft*, Vol. 29, No. 2, 1992, pp. 243–249.

[3]Linton, S. W., "Computation of the Poststall Behavior of a Circulation Controlled Airfoil," *Journal of Aircraft*, Vol. 31, No. 6, 1994, pp. 1273–1280.

[4]Davenport, F. J., and Hunt, D. N., "Deflection of a Thick Jet by a Convex Surface: A Practical Problem for Powered Lift," AIAA Paper 75-167, Jan. 1975.

[5]Takanashi, S., and Sawada, K., "Numerical Simulation of Compressible Flow Field About Complete ASKA Aircraft Configuration," Society of Automotive Engineers, TP 872346, Dec. 1987.

[6]Wille, R., and Fernholz, H., "Report on the First European Mechanics Colloquium, on the Coanda Effect," *Journal of Fluid Mechanics*, Vol. 23, Pt. 4, 1965, pp. 801–819.

[7]Fernholz, H. H., "Aerodynamische Hysterese, Steuerschneiden- und Reynoldszahl-Einfluß bei der Strömungsumlenkung und Ablösung an stark gekrümmten Wänden (Coanda Effekt)," *Zeitschrift für Flugwissenschaften*, Vol. 15, No. 4, 1967, pp. 136–142.

[8]Wilson, D. J., and Goldstein, R. J., "Turbulent Wall Jets with Cylindrical Streamwise Surface Curvature," *Journal of Fluids Engineering*, Vol. 98, No. 3, 1976, pp. 550–557.

[9]Bevilaqua, P. M., and Lee, J. D., "Design of a Supersonic Coanda Jet Nozzle," AIAA Paper 84-0333, Jan. 1984.

[10]Cornelius, K. C., and Lucius, G. A., "Physics of Coanda Jet Detachment at High-Pressure Ratio," *Journal of Aircraft*, Vol. 31, No. 3, 1994, pp. 591–596.

[11]Roe, P. L., "Approximate Riemann Solvers, Parameter Vectors and Difference Schemes," *Journal of Computational Physics*, Vol. 43, No. 1, 1981, pp. 357–372.

[12]Baldwin, B. S., and Lomax, H., "Thin Layer Approximation and Algebraic Model for Separated Turbulent Flows," AIAA Paper 78-257, Jan. 1978.

[13]Obayashi, S., Matsushima, K., Fujii, K., and Kuwahara, K., "Improvements in Efficiency and Reliability for Navier-Stokes Computations Using the LU-ADI Factorization Algorithm," AIAA Paper 86-0338, Jan. 1986.

[14]Sawada, K., "A Cell-Group Splitting Explicit Time Marching Scheme for Viscous Compressible Flows," *Proceedings of the International Symposium on Mathematical Modeling of Turbulent Flows*, Japan Society of Computational Fluid Dynamics, Tokyo, 1995, pp. 303–308.

[15]Goldberg, U. C., and Ramakrishnan, S. V., "A Pointwise Version of Baldwin-Barth Turbulence Model," *International Journal of Computational Fluid Dynamics*, Vol. 1, No. 4, 1993, pp. 321–338.